Performance of the advanced photon source 1-BM beamline optics

J. C. Lang,[a] G. Srajer, J. Wang, and P. L. Lee
Advanced Photon Source, Argonne National Laboratory, Argonne, Illinois 60439

(Received 30 June 1999; accepted for publication 10 September 1999)

Bending magnet beamlines at third-generation synchrotron sources combined with well-designed optics offer unique capabilities for providing high x-ray fluxes into relatively small focal spots. This article provides a description of the x-ray optics used in the Advanced Photon Source 1-BM beamline. The performance of these optics in terms of the delivered flux (9×10^{11} ph/s/100 mA at 10 keV), energy resolution [$\Delta E/E\approx1.5\times10^{-4}$ with Si(111)], and focusing properties (spot size $\approx0.25\times0.60$ mm) is compared with that expected from ideally reflecting and shaped optics.
[S0034-6748(99)03612-6]

I. INTRODUCTION

The primary motivation for the construction of third-generation synchrotron radiation facilities has been to increase the availability of high-brilliance insertion device beamlines. A somewhat neglected fact, however, has been that the bending magnets on these low-emittance storage rings can also offer high-quality x-ray beams suitable for a wide variety of experiments. In order to take full advantage of all the photons in a particular bandwidth provided by these bending magnet sources, however, focusing of the beam is absolutely essential. Focusing the bending magnet (BM) beam, at a third-generation source poses some unique challenges, since the distances from the source are large, thereby requiring larger optics than those used previously at other synchrotrons. The rewards for using these optics are quite substantial, though, since focusing enhances the x-ray flux on the sample by several orders of magnitude, with the flux density at the focal spot approaching that of an unfocused insertion device. This article briefly reviews the design principles of SRI-CAT 1-BM beamline at the Advanced Photon Source (APS). The measured performance of each of the optics used on this beamline is compared with that expected from ideally shaped optics.

APS bending magnet sources have a relatively high critical energy of 19.53 keV, therefore offering a useful spectral range from energies below 5 keV to energies greater than 100 keV. Furthermore the small source size on APS bending magnets, $\sigma_x=260$ μm and $\sigma_y=110$ μm [full width half maximum (FWHM)], is ideal for producing small focal spots. The horizontal fan of each APS bend magnet extends over 6 mrad, but front end apertures typically limit the maximum accepted beam to ~3.5 mrad on most beamlines due to size constraints on the optics and the beam transport pipes. Beamline 1-BM is a highly flexible beamline that has been used for a variety of experiments, such as diffraction, reflectivity, extended x-ray absorption fine structure (EXAFS), and high-energy scattering. The design of 1-BM is a combination of several successful beamline designs used previously at second-generation synchrotrons.[1–3] The beamline consists of three stations, A, B, and C, with only the later two used for experiments. The major optical components are two cylindrically bent mirrors and two alternately used focusing monochromators (Fig. 1). The first optical component is a water-cooled 1.2-m-long palladium-coated mirror located 25.5 m from the source. The x-ray beam is incident on this mirror at an angle of 2.8 mrad making the critical energy 24 keV. At this angle the mirror subtends 132 μrad vertically, thereby intercepting over 2/3 of total beam at 10 keV. This mirror is cylindrically bent in order to vertically ''collimate'' the beam (i.e., focus the beam at infinity). Collimating the beam allows the user to accept a larger portion of the vertical beam without sacrificing any energy resolution, because all the rays in the beam after the mirror will make a nearly identical angle with any vertically diffracting monochromator crystal further downstream. The collimating mirror is followed by the double-crystal monochromator (DCM). The second crystal in the DCM is a sagittally bent crystal, which provides horizontal focusing of the beam into the C station. Si(111), Si(220), and Si(400) crystals have been fabricated for this monochromator, which give it energy ranges of 4–25, 6–39, and 8–58 keV, respectively. If the first crystal of the DCM is translated out of the beam, the third optical component, a dispersive monochromator located in the B station of the beamline, can be used. This monochromator horizontally diffracts and meridionally focuses the beam into this station providing a polychromatic beam used primarily for time-resolved dispersive EXAFS or diffraction measurements for energies between 5 and 20 keV. By using crystals with a small asymmetry and moving the collimating mirror out of the beam, this monochromator can also be used to focus monochromatic radiation in the 40–80 keV range inside the B station. When passing the beam into the C station, the dispersive monochromator can be translated out of the beam. The last optical component in the beamline is a 1-m-long palladium-coated cylindrical mirror located between the B and C stations. This mirror provides vertical focusing of the beam for the C station. The incident angle on this mirror is adjustable up to 5.6 mrad, although in normal operation it remains at 2.8 mrad in order to provide a horizontal beam into the C station. This mirror can also be moved out of the beam path, and the collimating mirror can be used to focus the beam into the C station if so desired.

[a]Electronic mail: lang@aps.anl.gov

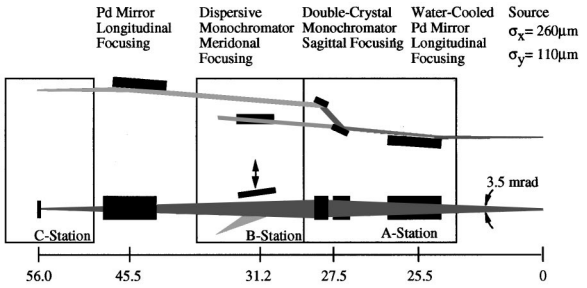

FIG. 1. Top and side view schematic of the major optical components on the 1-BM beamline indicating their distance (meters) from the source and the location of the experiment stations. The size of the source is given in microns (FWHM).

These optics offer the 1-BM user great flexibility in optimizing the conditions for their experiments. For instance, the 1-BM-B experiment station can provide the user with white beam (all energies), pink beam (mirror reflected), and monochromatic beam from either monochromator, both with and without the collimating mirror in the beam. Furthermore, the focal distance from the monochromators can be adjusted to various positions within the station. The 1-BM-C station offers the user a doubly focused beam between 5 and 24 keV. When taking beam into the C station, the collimating mirror must be in place since the vertical displacement of the beam from this mirror requires raising the entire beam transport between the experiment stations to accommodate it.

II. OPTICAL COMPONENTS

A. Collimating mirror

The collimating mirror was fabricated by Carl Ziess (Germany) on a Si substrate with specification of 3 Å surface roughness and <4 μrad meridional surface slope errors (including thermal effects) over a range of spatial frequencies from 2 to 1100 mm. The cylindrical bend on this mirror can be continuously adjusted from a flat profile to a radius of 7 km using a pneumatic bending mechanism.[4] The performance of this mirror was checked in two ways. First, a simple calibration was made of the bending radius of the mirror versus the applied pressure on the pneumatic bender by measuring the beam size in both the B and C stations. Second, to measure the mirror's effects on the beam divergence, a highly dispersive reflection from a Si crystal ''analyzer'' was placed after the DCM. The rocking curve width of this reflection is directly related to the bandpass of the monochromator and thus the divergence after the mirror. The bandpass of flat-crystal optics used in the DCM is given by

$$\frac{\Delta E}{E} = \sqrt{\Omega^2 + \omega_D^2}\,\cot\theta_B\,, \tag{1}$$

where Ω is the angular spread of the beam in the diffraction plane, ω_D is the Darwin width of the diffracting crystal, and θ_B is the Bragg angle. Our measurements at 10 keV showed that, for a beam with a 109 μrad vertical divergence incident on the mirror, the bandwidth was reduced from 5.5×10^{-4} to 1.5×10^{-4} for Si(111) and from 3.6×10^{-4} to 8.1×10^{-5} for Si(220), when the mirror bend was changed from flat to collimating. The lower values on the energy resolution are 15% and 25% above the theoretical limit (i.e., perfect collimation, $\Omega\approx0$) and indicate that the beam after the mirror had a minimum vertical divergence of ~10 μrad. Spherical aberrations from the mirror due to its non-ellipsoidal shape (~1 μrad) and the finite extent of the source (~5 μrad) account for some of this residual divergence, but the predominant source was found to be slope errors in the figure of the mirror on the order of 10 μrad. This was confirmed by scanning the mirror through a small x-ray beam and noting the position of the analyzer crystal reflection. The position of the reflection is directly correlated to the angle of the incident beam, thereby it can be used to obtain a profile of the mirror in its bent state. This measurement showed that, while the central 0.8 m of the mirror had only 2–3 μrad deviations from an ideal bend, both of the edges of the mirror were substantially overbent to the 10 μrad figure above. Confining the incident beam to only the central portion of the mirror, we were able to obtain a post-mirror vertical divergence almost entirely determined by the particle beam source size, albeit with a loss in overall flux.

B. Double-crystal monochromator

The DCM on the 1-BM beamline was manufactured the Physical Sciences Laboratory at the University of Wisconsin. The monochromator design is ultrahigh vacuum (UHV) compatible with no motors inside the vacuum, and all motions accomplished through bellowed actuators.[5] It is a fixed-exit monochromator design (35 mm offset) with two translations and one rotation for selecting the energy. The main rotation axis (θ) lies at the intersection of the surface normal of the first crystal and the plane defined by the surface of the second crystal. The first crystal is indirectly cooled by placing it in contact with a water-cooled copper manifold using an In–Ga eutectic. When used in conjunction with the collimating mirror, which also acts as a power filter, this cooling method provides effective cooling of the crystal optics with observed thermal broadening of the monochromator rocking curve of less than 1 arcsec for 100 mA of beam current. The monochromator has proved extremely stable for fixed-energy experiments, with parallelism losses between the two monochromator crystals limited to less than 1/2 arcsec over the course of several fills during a week of running. When this monochromator is used without the collimating mirror in place, however, the additional Compton-scattered radiation puts a greater thermal load on the crystal mounting stages. This results in parallelism losses between the crystals when the beam is first incident on the monochromator. After approximately 10 min, the monochromator reaches thermal equilibrium and minimal thermal drifts are observed during the remainder of the fill. Future plans to operate the APS at a constant particle beam current should greatly minimize these effects.

The design of the sagittal crystal on the DCM, illustrated in Fig. 2, was first proposed by Kushnir *et al.*[6] The crystal is fabricated in a U shape with a large thin ($0.5\times80\times114$ mm) top portion and two thicker legs ($5\times10\times114$ mm). The bending mechanism applies pressure on the legs of the crys-

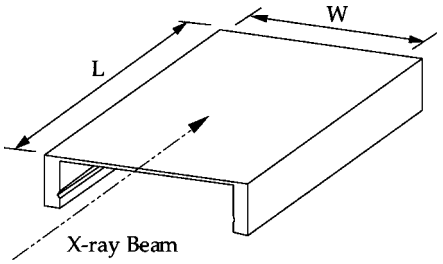

FIG. 2. Design of the sagittal focusing crystal showing the thicker legs used to hold and bend the crystal and the thin diffracting portion cut in the golden aspect ratio.

tal via PZT actuators pushing them apart thereby bending the top portion into a cylindrical shape.[7] The novel design of this optic is in the fact that no thicker portions of crystal (stiffening ribs) are needed along the length of the crystal to prevent anticlastic bending.[8] Anticlastic bending is unwanted bending in the diffraction plane of the crystal as the crystal is bent in the sagittal direction transverse to the beam. This sagittal crystal design eliminates the need for ribs by choosing the length-to-width ratio to be in a so-called ''golden ratio'' (1.42 in our case) determined by U-shaped geometry and the Poisson coefficient for the monochromator material. We should note that although Ref. 6 only presented a golden ratio calculation for a Si(111) crystal where the Poisson coefficient is nearly isotropic in the diffraction plane. It has been found, though, that the determining factor in calculating the value of the golden ratio is the constraint placed on the thin diffracting portion of the crystal by the thicker legs, therefore monochromator crystals utilizing different Bragg reflections also can be cut using the same 1.42 golden ratio.[9]

The performance of the bender/sagittal crystal was first measured using a Si(220) reflection. Figure 3 shows the horizontal focus of 0.45 mm (FWHM) achieved at 10 keV for a 72 mm (2.62 mrad) wide beam incident on the monochromator. The rocking curve width of the Si(220) reflection for a focused beam of this size was measured to be only 25% above that of an ideal case for a flat crystal. One worrisome problem with the focus shown in Fig. 3 is the long tail toward the inboard side. By scanning a small beam horizontally across the monochromator crystal, we found that this tail came from only a 10 mm portion of the crystal near one

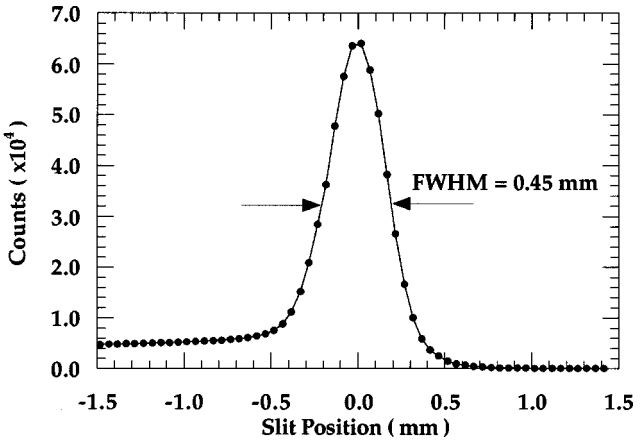

FIG. 3. Horizontal focal size (FWHM) for the Si(220) sagittal focusing crystal.

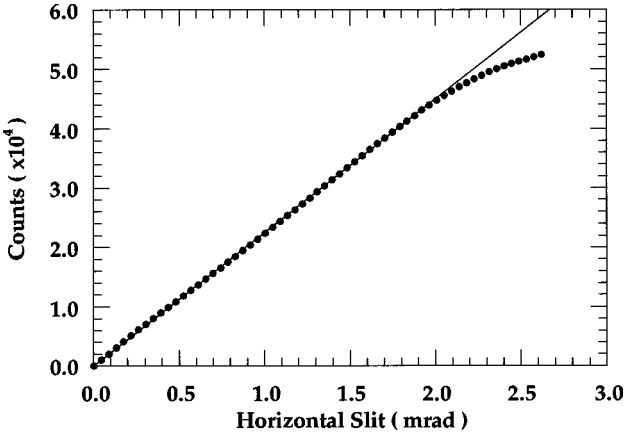

FIG. 4. Linearity of observed counts in C station for increasing horizontal slit size using a Si(111) sagittal focusing crystal.

of the legs. We believe that this aberration is due to nonuniform thickness of the sagittal crystal. While great care was taken to polish the top diffracting surface, the surface underneath was just machine ground and etched, which resulted in 10–15% thickness variations. New crystals are in the process of design and fabrication to try to improve the focus. Another measure of the performance of this crystal is shown in Fig. 4, which plots the flux obtained in the C station focus as the horizontal size of the beam incident on the monochromator is increased. Note that the increase is nearly linear for beam divergences lower than 2 mrad. Subsequent tests with Si(111) crystals have yielded similar results.

C. Dispersive monochromator

A detailed description of the dispersive monochromator has been previously given by Brauer *et al.*;[10] therefore only a brief description of its performance will be given here. This monochromator provides polychromatic radiation primarily used for time-resolved near-edge and EXAFS absorption measurements. The size of the horizontally focused beam from this monochromator is approximately 100 μm (FWHM) with the vertical size determined by the defining slits. The incident beam size, focusing radius of the monochromator, and position of the detector can be varied to obtain the desired bandwidth, which can range from 0.1 to 0.9 keV, the lower limit being fixed by the size of the experiment station and the upper limit by the monochromator working distance. Figure 5 shows an absorption measurement of the Cu *K* edge taken in 7 ms taken using a Si(220) monochromator crystal and a phosphor-coupled charge-coupled device (CCD) detector. The energy resolution for this measurement was estimated to be ~5.5 eV by comparing this spectra with that taken using a conventional scanning monochromator. The energy resolution in this measurement is limited by the effective pixel size of the CCD detector and can be improved by simply moving the detector further from the focus although this sacrifices some of the energy range.

D. Vertically focusing mirror

The vertically focusing mirror was manufactured by SESO (France) on a zerodur substrate. The specified surface

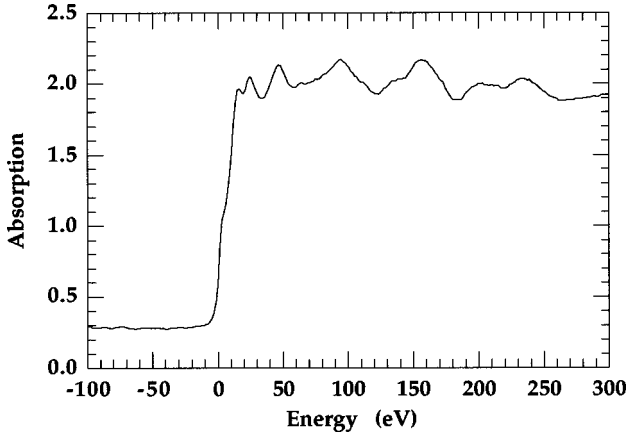

FIG. 5. Measurement of the Cu *K* edge taken in 7 ms using the dispersive monochromator with a Si(220) crystal.

roughness and slope errors were 3 Å and 6 μrad (rms) in the same wavelength band as for the collimating mirror. The cylindrical bend on this mirror can be adjusted from flat to a 3.5 km radius using a microstepped motor inside the mirror vacuum tank. This mirror reflects the beam downward; thus if the incident angle is set at 2.8 mrad to match the angle of the collimating mirror, the beam entering the C station is horizontal. The angle can be increased, however, if harmonic rejection is required at lower energies. The performance of this mirror was first checked by scanning a 50 μm slit through the beam as the mirror was focused and using flat crystal optics in the DCM monochromator. Figure 6(a) shows the minimum vertical beam size achieved for a 87 μrad beam incident on the first mirror (bent to the collimating radius. The 108 μm (FWHM) focus size achieved compares quite well with the expected value of 88 μm.

Although we were able to achieve a good focus, a great deal of structure was observed in the unfocused beam, shown in Fig. 6(b). This structure occurs in straight lines across the mirror surface transverse to the beam direction. Similar beam features have been observed from other mirrors installed at third-generation beamlines and were ascribed to effects of the beam coherence. In our case, however, this does not seem to be predominant cause of the structure, since only minimal changes in the structure are observed for different incident beam energies. The structure here seems to arise simply from slope errors in the figure of the mirror. Figure 7 shows a measurement of these slope errors made by moving the mirror through a small beam and recording the position of the reflected beam in the C station with a CCD camera. Besides the large 10 μrad deviations on either edge, there are regular 2–3 μrad errors across the entire surface The predominant frequencies of these slope errors occur at 17 and 25 mm along the mirror surface. These are nearly identical to those obtained from optical interferometry measurements of the mirror surface prior to installation.[11] The slope errors alternately focus and defocus the beam thereby producing the observed striped structure. The collimating mirror on the beamline, which had slope errors of similar magnitude, did not display structure as dramatic as this because the deviations in the slope from an ideal figure for that mirror occurred over a much longer spatial frequency on the mirror

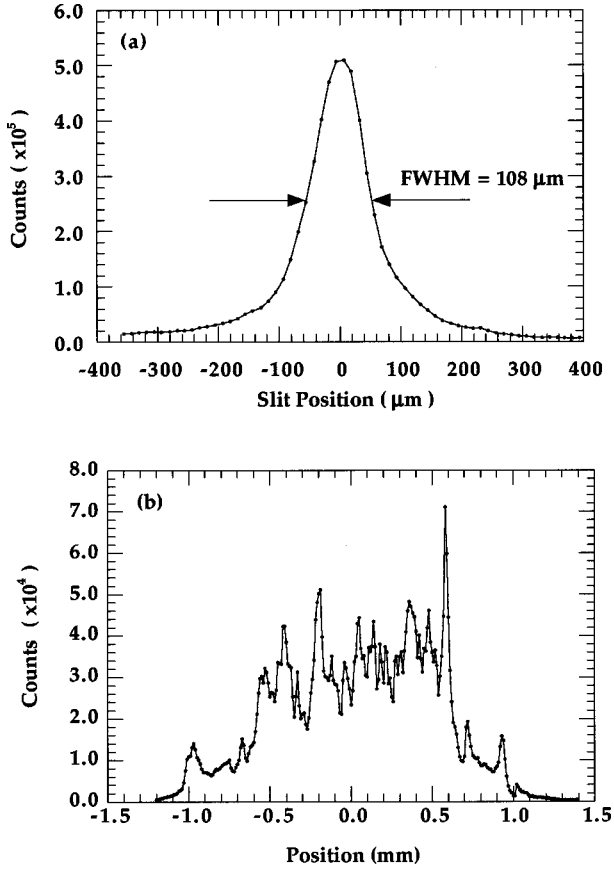

FIG. 6. (a) Vertical focal size (FWHM) for the focusing mirror using an unfocused horizontal beam, (b) beam structure observed for an unfocused beam.

surface. One should note, though, that the magnitude of these slope errors is within the specifications and is at the limit of current mirror polishing technology for mirrors of this size. Such features as those described have been observed on mirrors from a number of different manufacturers and on a variety of substrates. The reason that these features are more prominent at a third-generation source as opposed to at pre-

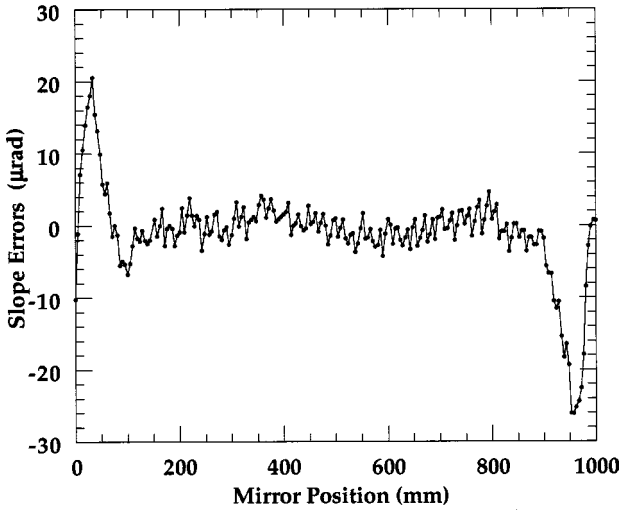

FIG. 7. Measured slope errors in the focusing mirror as a function of mirror position.

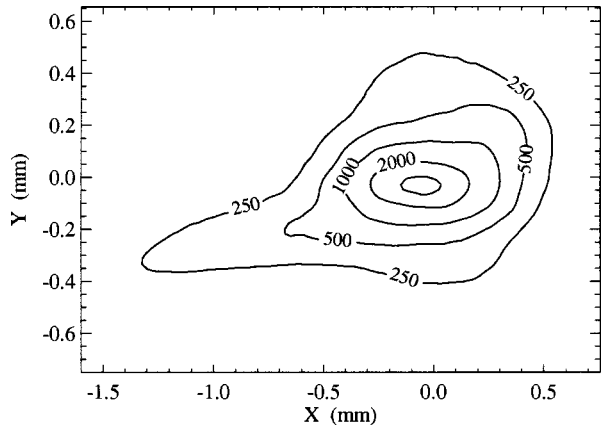

FIG. 8. CCD image of the doubly focused beam in the C station using both mirrors and a Si(111) monochromator crystal. Contours are arbitrary units corresponding to the number of counts in the CCD detector.

vious synchrotrons is that the small source size coupled with the large beamline distances greatly increase the vertical angular resolution. Future improvements in mirror polishing are needed to preserve the full brilliance of the x-ray beam at third-generation facilities.

III. COMBINED PERFORMANCE

A summary of the combined performance of all the optics is contained in Figs. 8 and 9. Figure 8 shows a CCD image of a doubly focused 9.0 keV beam in the C station using a Si(111) monochromator. This spot size was focused with a 2.20 mrad $H\times 0.09$ mrad V beam incident on the monochromator. Profiles of this image give FWHM values of 0.25 mm vertical and 0.60 mm horizontal. These values are roughly twice as large as those obtained using ray tracing, assuming ideally shaped cylindrical focusing optics. The increase in the vertical spot size compared to that taken with flat crystal optics is believed to be due to aberrations induced by a slight twisting in the sagittal crystal. While the increase in the horizontal focal size is probably due to nonuniformities in the thickness of the sagittal crystal as discussed above. Another thing to note is that the focused beam has a long diffuse tail with ~5% of the peak intensity. Thus, a series of defining slits needs to be placed along the beam, especially near the focus, for experiments with small scattering angles. Most of the contribution to these tails arises from the portions of the crystals near the legs of the sagittal crystal. If the incident beam is reduced to 1.75 mrad H, this tail can be nearly eliminated.

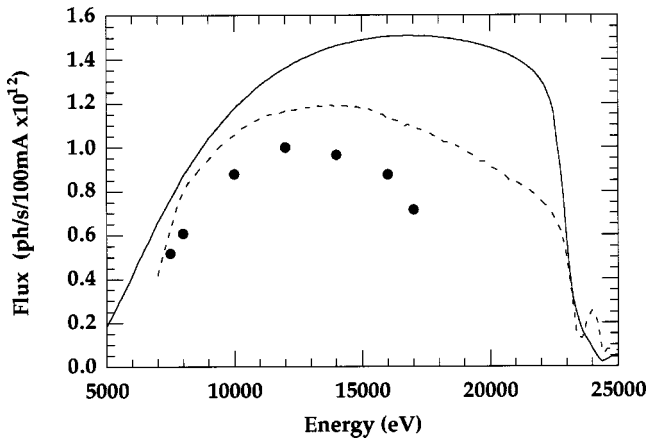

FIG. 9. Theoretical flux (solid) for a 1.75 mrad $H\times 0.09$ mrad V beam with a Si(111) monochromator and the observed flux with flat crystals (dash) and the fully focused sagittal crystal (circles).

Figure 9 gives the achieved photon fluxes into such a focus for a series of energies along with that achieved for the same size beam with flat crystals measured in the B station and the flux expected from perfect crystal optics. Both the flat and bent crystal optics deviate from the ideal optics curve at higher energies. This is believed to be due strain or thermal effects in the DCM crystals, which are more prominent relative to the Darwin width of the monochromator crystals for higher energies. In the case of the flat crystal, the effects of thermal heating on the first crystal are probably the cause, while for the sagittal crystal the steeper drop off is probably due to the increasing strain of bending the crystal to the smaller bending radii required for increasing energy. We should note that, in principle, the optics can accept even larger beams, but we have given the flux for this size beam since it yielded a reasonable focus and bandwidth. If these factors are not critical to the experiment, the maximum beam size (3.00 mrad $H\times 0.13$ mrad V) can be used to increase the expected flux to 2.5×10^{12} ph/s/100 mA at 10 keV. For this case, the focus assumes an irregular shape with most of the flux in a 0.3 mm vertical and 0.7 horizontal spot and a diffuse tail (~5% of peak intensity) extending for approximately 5 mm.

IV. COMPARISON WITH AN INSERTION DEVICE BEAMLINE

It is instructive to compare these values with those obtained from an insertion device (ID) beamline. For instance, a 1×1 mm^2 unfocused beam 65 m from the source from a standard APS undulator A[12] using a Si(111) monochromator would in theory yield 1.0×10^{13} ph/s/100 mA at 10 keV,[13] only an order of magnitude above the observed flux on 1-BM into a well-defined focus. We should also note, that because of the collimation of the beam prior to the monochromator, the bandwidths on 1-BM are nearly the same as those seen on the ID beamlines. If focusing optics are used to collect the entire central cone of the undulator beam, this flux differential increases to a factor of 40. This comparison between a BM and ID source demonstrates that the great strength of ID devices is primarily the brilliance provided and not necessarily their overwhelming flux. Thus, for experiments that require only a large incident flux on the sample with relaxed conditions on the beam collimation, a BM beamline can be a viable alternative to an ID beamline.

ACKNOWLEDGMENTS

The authors would like to thank Bill McHargue for countless hours put in constructing this beamline and to Dennis Mills for invaluable suggestions concerning the design and testing of this beamline. This work is supported by the U.S. DOE-BES under Contract No. W-31-109-ENG-38.

[1] A. Habenschuss, G. E. Ice, C. J. Sparks, and R. A. Neiser, Nucl. Instrum. Methods Phys. Res. A **266**, 215 (1988).
[2] W. J. Trela, R. J. Bartlett, F. D. Michaud, and R. Alkire, Nucl. Instrum. Methods Phys. Res. A **266**, 234 (1988).
[3] P. L. Lee, M. A. Beno, G. Jennings, M. Ramanathan, G. S. Knapp, K. Huang, J. Bai, and P. A. Montano, Rev. Sci. Instrum. **65**, 1 (1994).
[4] D. Pauschinger, K. Becker, and R. Ludewig, Rev. Sci. Instrum. **66**, 2177 (1995).
[5] F. H. Middleton, G. R. Emmel, F. Feyzi, and G. M. Gregerson, Rev. Sci. Instrum. **67**, 3351 (1996).
[6] V. I. Kushnir, J. P. Quintana, and P. Gerorgopoulos, Nucl. Instrum. Methods Phys. Res. A **328**, 588 (1993).
[7] P. Zschack, G. E. Ice, and D. J. Robinson (unpublished).
[8] C. J. Sparks, G. E. Ice, J. Wong, and B. W. Battermann, Nucl. Instrum. Methods **194**, 73 (1982).
[9] J. P. Quintana (private communication).
[10] S. Brauer, B. Rodricks, L. Assoufid, M. A. Beno, and B. Knapp, Rev. Sci. Instrum. **67**, 3349 (1996).
[11] L. Assoufid, J. C. Lang, J. Wang, and G. Srajer, Proc. SPIE **3347**, 109 (1998).
[12] R. J. Dejus, B. Lai, E. R. Moog, and E. Gluskin, Report ANL/APS/TB-17 Argonne National Laboratory, IL 60439.
[13] R. J. Dejus and M. Sanchez del Rio, Rev. Sci. Instrum. **67**, 3356 (1996).